Synthesis and Characterization of Boron Azadipyrromethene Single-Wall Carbon Nanotube Electron Donor−Acceptor Conjugates

Kevin Flavin,[†] Katherine Lawrence,[‡] Juergen Bartelmess,[‡] Mariusz Tasior,[§] Cristina Navio,[⊥] Carla Bittencourt,[⊥] Donal F. O'Shea,[§] Dirk M. Guldi,[‡] and Silvia Giordani[†,*]

[†]School of Chemistry/CRANN, Trinity College Dublin, College Green, Dublin 2, Ireland, [‡]Department of Chemistry and Pharmacy & Interdisciplinary Center of Molecular Materials (ICMM), Friedrich-Alexander-University Erlangen-Nuremberg, Egerlandstrasse 3, 91058 Erlangen, Germany, [§]Centre for Synthesis and Chemical Biology, School of Chemistry and Chemical Biology, University College Dublin, Belfield, Dublin 4, Ireland, and [⊥]University of Mons, Parc Initialis, Avenue Nicolas Copernic 1, Mons 7000 Belgium

ABSTRACT The preparation of a novel donor−acceptor material, consisting of a red/near-infrared (NIR) absorbing boron azadipyrromethene donor covalently attached to a highly functionalized single-wall carbon nanotube (SWNT) acceptor, which bears great potential in the field of organic photovoltaics, has been demonstrated. Both purification and covalent functionalization of SWNTs have been demonstrated using a number of complementary characterization techniques, including atomic force microscopy, Raman, X-ray photoelectron spectroscopy (XPS), Fourier transform infrared, and NIR-photoluminescence spectroscopy, and a functionalization density of approximately 1 donor molecule per 100 SWNT atoms has been estimated by XPS. The redox behavior of the fluorophore has been investigated by electrochemistry and spectroelectrochemistry as well as by pulse radiolysis. The donor−acceptor properties of the material have been characterized by means of various spectroscopic techniques, such as UV−vis NIR absorption spectroscopy, steady-state and time-resolved fluorescence spectroscopy, and time-resolved transient absorption spectroscopy. Charge transfer from the photoexcited donor to the SWNT acceptor has been confirmed with a radical ion pair state lifetime of about 1.2 ns.

KEYWORDS: carbon nanotubes · functionalization · near-infrared fluorophore · donor−acceptor conjugate · transient absorption spectroscopy

In recent years, diminishing natural resources and increased energy demand has lead many research groups to focus their attention on the development of environmentally clean alternative energy resources.[1] Particular emphasis has been placed on solar energy conversion, where research fields have emerged targeting both photocatalysis for the production of clean fuels[2] and mimicking of photosynthesis using donor−acceptor-based assemblies and materials.[3]

Functionalization of carbon-based nanomaterials has recently received an enormous amount of attention for a variety of applications.[4−7] In particular fullerenes and single-wall carbon nanotubes (SWNTs) have been of great interest with regards to their use as acceptors in donor−acceptor systems stemming from their natural electron-acceptor ability.[8] Straightforward delocalization of transferred electrons through these highly conjugated structures results in low reorganization energies, ultrafast charge separation, and slow charge recombination, making them ideal candidates for optoelectronic applications.[9]

SWNTs also demonstrate further unique properties, such as high electrical conductivity,[10] tensile strength,[11] and chemical stability,[12] that further enhance their potential and has led to many reports demonstrating their use as both nanoconjugates (donor covalently attached) and nanohybrids (donor noncovalently attached). A variety of donor molecules have been investigated, such as tetrathiafulvalene,[13] ferrocene,[14] and ruthenium bipyridine complexes,[15] however large attention has been given to porphyrins[16−20] and related phthalocyanines,[21−23] due to their excellent optical and electronic properties. Among these donor molecules only the latter, phthalocyanines, demonstrates intense absorption in the red/near-infrared region of the spectrum, which is of major importance with regards to improving light-harvesting performance for photovoltaic applications. One drawback of phthalocyanines, however, is that they often suffer from poor solubility. This is a problem often encountered with the development of new NIR fluorophores, in addition to further possible drawbacks, such as aggregation, photobleaching, photoinstability, and low quantum yields.[24]

*Address correspondence to giordans@tcd.ie.

Received for review October 20, 2010 and accepted January 8, 2011.

Published online 10.1021/nn102831x

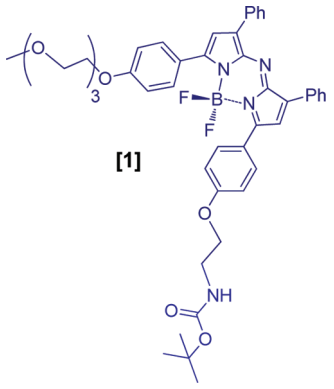

Figure 1. Conjugatable boron-chelated tetraarylazadipyrromethene [1].

Boron-chelated tetraarylazadipyrromethenes are a novel class of red/near-infrared fluorophores that have recently been developed,[25,26] which may be synthesized relatively easily, are amenable to structural modification, and exhibit excellent spectral properties, such as high extinction coefficients (70 000−80 000 M^{-1} cm^{-1}) and large fluorescence quantum yields above 700 nm.[27] These appealing attributes have led to their adaption for use in applications, such as fluorescent sensing[28,29] and as photosensitizers in photodynamic therapy,[25,30] and show definite promise for their applicability in photovoltaics.

In the current study we describe the covalent conjugation, *via* amide-bond formation, of the amine functionalized NIR fluorophore [**1**] (Figure 1) with SWNTs and subsequently investigate the charge-transfer properties between the tetraarylazadipyrromethene unit and the highly functionalized SWNT acceptor. A number of spectroscopic techniques, including NIR photoluminescence (NIR-PL), Raman, Fourier transform infrared (FTIR), UV−vis absorption and emission, and X-ray photoelectron spectroscopy (XPS), were used to demonstrate successful purification and functionalization of the samples. Steady-state and time-resolved fluorescence spectroscopy in addition to time-resolved transient absorption spectroscopy were subsequently used to demonstrate charge transfer from the photoexcited donor to the SWNTs.

RESULTS AND DISCUSSION

The synthetic procedure for the preparation of fluorophore [**1**] conjugated SWNTs (f-SWNTs [**5**]) is illustrated in Scheme 1. Initially raw SWNTs (r-SWNTs [**2**]) were purified by successive treatments with nitric acid, sodium hydroxide, and hydrogen peroxide in order to remove unwanted catalyst and carbonaceous material from the sample. This purified material (p-SWNTs [**3**]) was covalently functionalized, using a procedure developed by Tour and co-workers,[31,32] where successive treatments with *in situ* generated 4-carboxybenzenediazonium produced highly functionalized and easily dispersible f-SWNTs [**4**]. Fluorophore [**1**] was synthesized as previously described,[27] deprotected using trifluoroacetic acid (Scheme S1, Supporting Information) and coupled to f-SWNTs [**4**] following conversion of the benzoic acid groups to the corresponding electrophilic acid chloride moieties.

The functionalization procedure was followed by Raman spectroscopy, and the spectra following each synthetic step are shown in Figure 2. It is evident that only slight changes in the RBM, G, and 2D bands are observed. The D band on the other hand, activated by the presence of defects on the nanotube surface,[33] is clearly affected, where the D/G ratio is reduced following purification and substantially enhanced following the Tour functionalization, indicating covalent functionalization. Background emission is evident from the spectrum when excited at 633 nm following attachment of [**1**], and a peak characteristic of the C═C and C═N in plane vibration of the pyrrole rings in the azadipyrromethene can be seen at approximately 1420 cm^{-1} (Figure 2B).

The functionalization procedure was also monitored by XPS following the C 1s spectrum (Figure 3), where the table shows fitting of the peak into its various components. Characteristic contributions from the primary graphitic peak (284.4 eV) and plasmon loss

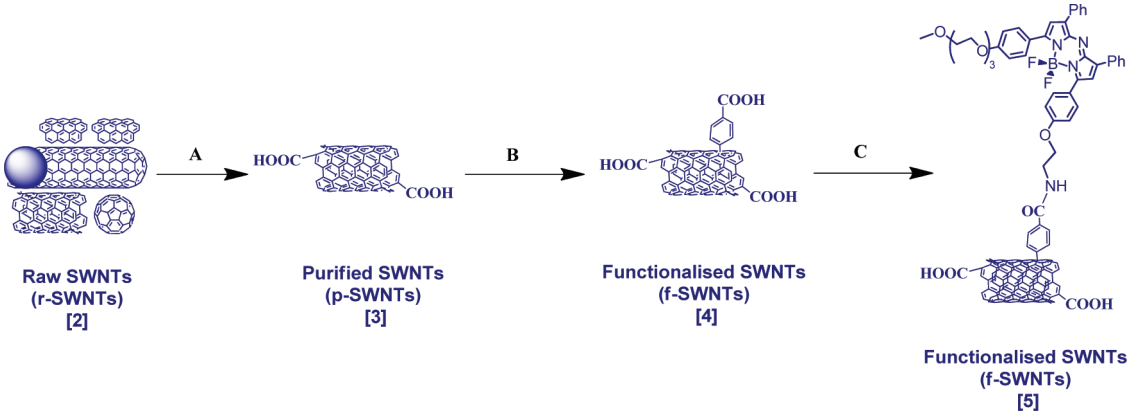

Scheme 1. Synthesis of boron azadipyrromethene SWNT conjugate: (A) purification, (B) functionalization with benzoic acid groups, and (C) attachment of fluorophore [1].

(290.6 eV) are present in r-SWNTs. Following the oxidative purification procedure, as expected two new peaks appear that relate to the increasing sp^3 content (285.3 eV) and the introduction of oxygen containing groups (288.8 eV) onto the nanotube structure. Upon treatment with the diazonium compound to form f-SWNTs [**4**] there is the appearance of a new peak at 288.1 eV related to the attached benzoic acid groups.[34] This is accompanied by the disappearance of the plasmon loss suggesting covalent functionalization of the nanotube side wall. In the final sample, f-SWNTs [**5**], further peaks appear in combination with an additional increase in the sp^3 character resulting from conjugation of [**1**].

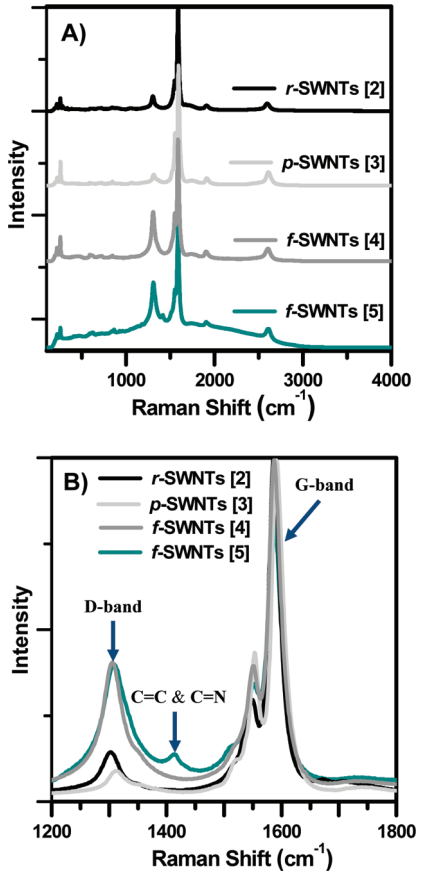

Figure 2. Raman spectra recorded after excitation at 633 nm from the raw, purified, and functionalized SWNTs.

Figure 4 shows an XPS survey spectrum of the f-SWNTs [**5**] where, in addition to the peaks expected for the raw material, *i.e.*, the C 1s (284.4 eV) and the Auger lines carbon KLL (near 1200 eV) and oxygen KVV (near 1000 eV), the peaks generated by photoelectrons emitted from oxygen, nitrogen, fluorine, and boron atoms are also evident, confirming the presence of conjugated [**1**] in the sample. The efficiency of the functionalization was also estimated from the XPS data (Tables S1−3, Supporting Information). It was estimated from the O 1s peak that f-SWNTs [**4**] has approximately 1 benzoic acid group attached every 20 carbon nanotube atoms, in accordance with the literature,[35] and from the N 1s peak that f-SWNTs [**5**] has approximately 1 dye molecule attached every 100 carbon nanotube atoms. The B 1s peak was examined to determine whether the coupling reaction conditions had any effect on chelation of the boron, and given that there is 1 boron atom per 112 carbon nanotube atoms, we estimate that approximately 90% of the attached molecules of [**1**] are unaffected.

FTIR spectra of all nanotube samples are illustrated in Figure 5A in order to assess functional group introduction. Following the purification procedure very little change is evident, however after the diazonium treatment new absorption bands can be observed in the fingerprint region of the spectrum, notably the carbonyl stretching band near 1700 cm^{-1}. Following conjugation of [**1**], this band shifts in frequency, and its relative intensity decreases indicating conversion of

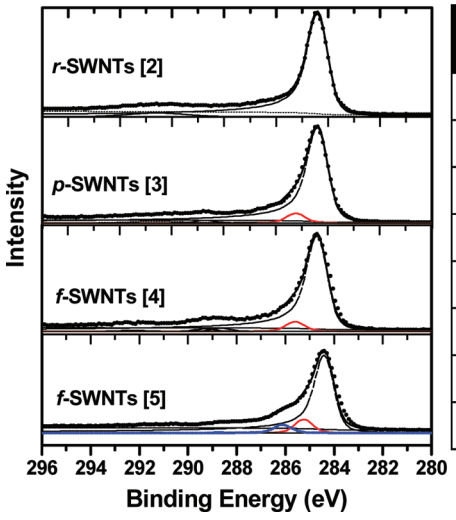

Binding Energy (eV)	r-SWNTs [2]	p-SWNTs [3]	f-SWNTs [4]	f-SWNTs [5]	
284,4	94,5%	90,0 %	90,5 %	82,5 %	sp^2
285,3	-	5,5 %	5,5 %	8,5 %	sp^3
286,1	0	0	0	5.00%	
287.2	0	0	0	1,0 %	
288,1	0	0	1,5 %	1,0 %	
288.8	0	2,0 %	1,5 %	1,0 %	
290,6	5,5 %	2,5 %	-	-	π-plasmon
291,5	-	-	1,0 %	1,0 %	

Figure 3. XPS C 1s spectrum of the raw, purified, and functionalized SWNTs. Table shows the binding energy of the different components used in the fitting and the relative concentration of each.

the acid to an amide, suggesting covalent attachment to the SWNTs.

NIR-PL measurements (Figure 5B) demonstrate that the SWNTs, although quenched, still demonstrate structured emission following purification. Diazonium treatment, however, results in complete loss of photoluminescent behavior, indicating covalent attachment of the benzoic acid groups to the side wall of the SWNTs,[36] in agreement with the XPS and Raman results. NIR-PL spectra were taken of each sample and dispersed in aqueous sodium dodecylbenzene sulfonate (SDBS) solution, and as expected, the dispersibility of the purified SWNTs was greatly increased following diazonium functionalization, and notably the color of the dispersion changed from a dark brown to a dark green following conjugation of [**1**] (Figure 5C).

The effect of purification and functionalization on the integrity of the SWNTs was investigated by AFM (Figure 6). On comparison of r-SWNTs [**2**] and p-SWNTs [**3**], it is evident that the purification procedure is successful in quantitatively removing catalyst and carbonaceous material from the sample, leaving behind SWNTs bundles. Following the functionalization procedures, it is clear that the f-SWNTs [**4**] and [**5**] have kept their integrity and that the samples are relatively clean as a result of the stringent washing procedures employed. Dispersibility of the functionalized samples is much improved, as is evident from both the aqueous SDBS dispersions (Figure 5C) and the AFM images

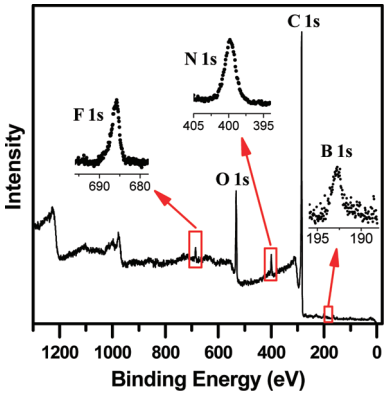

Figure 4. XPS spectrum of functionalized SWNTs [5].

(where all samples were prepared in an identical manner). This is of special interest for photovoltaics as one of the barriers to generating feasible photovoltaic devices, using longer nanotubes is their tendency to aggregate into insoluble bundles thus inhibiting processability.[9] Highly functionalized SWNTs alleviate this problem by reducing the effect of bundling and roping in the material.[37]

Steady-state absorption spectra of raw, purified, and functionalized SWNTs are displayed in Figure S1, Supporting Information, and it is clear that van Hove singularities are still present following purification, however, disappear following the Tour reaction as reported in the literature.[31] In f-SWNTs [**5**] maxima appear at 466 and 698 nm corresponding to the peaks observed for [**1**] at 462 and 697 nm (Figure 7). An overall broadening of the fluorophore assigned bands of f-SWNTs [**5**] suggests electronic communication between the constituents indicating covalent conjugation of [**1**] as opposed to physisorption. The latter conclusion is supported upon examination of the absorption spectrum when the dye is simply mixed with a dispersion of f-SWNTs [**4**], where the characteristic maximum is observed at 695 nm and no broadening relative to [**1**] is perceived.

Analysis of the steady-state emission spectrum, taken at an excitation wavelength of 450 nm, provides additional evidence for electronic communication between the SWNT and the fluorophore (Figure 8). Specifically, while [**1**] gives rise to a fluorescence quantum yield value of 0.49, f-SWNTs [**5**] demonstrate a quantitatively quenched fluorescence, implying rapid deactivation of photoexcited fluorophore [**1**].[23] Furthermore, while the reference fluorophore [**1**] has a fluorescence lifetime of 2.8 ns, f-SWNTs [**5**] did not reveal any appreciable change within the time resolution of 0.1 ns of our instrumental apparatus. Interestingly, a mixture of the reference fluorophore [**1**] and f-SWNT [**4**] demonstrated comparable fluorescence to the fluorophore alone.

To determine the exact nature of the electronic interactions, femtosecond transient absorption spectroscopy was employed. Upon laser excitation at 700 nm, the excited state characteristics of [**1**] give rise to

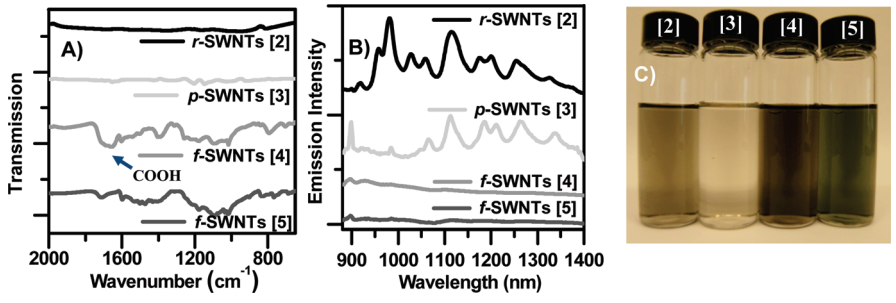

Figure 5. (A) Infrared spectra, (B) NIR-PL spectra, and (C) aqueous SDBS dispersions of the r-SWNTs [2], p-SWNTs [3], and f-SWNTs [4] and [5].

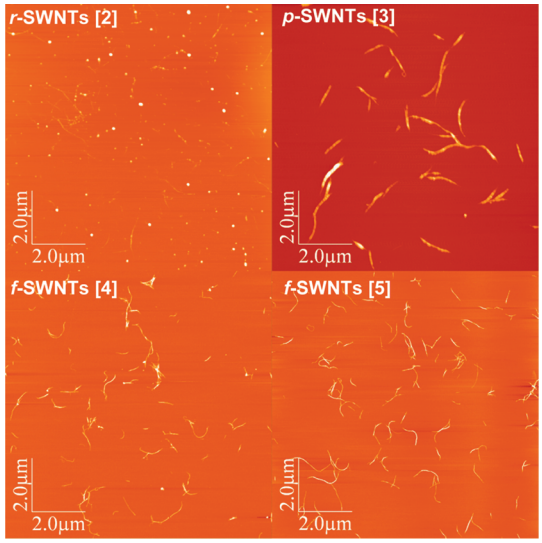

Figure 6. AFM images of small bundles of r-SWNTs [2] (z = 0−45 nm), p-SWNTs [3] (z = 0−30 nm), f-SWNTs [4] (z = 0−15 nm), and f-SWNTs [5] (z = 0−14 nm) on mica.

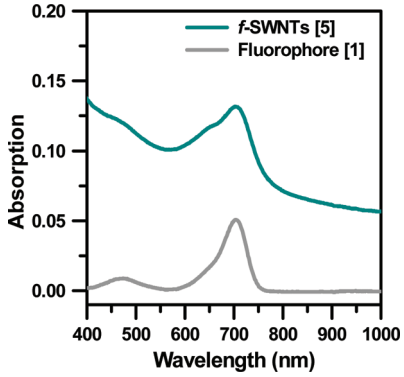

Figure 7. Steady-state absorption spectra of fluorophore [1] and f-SWNTs [5].

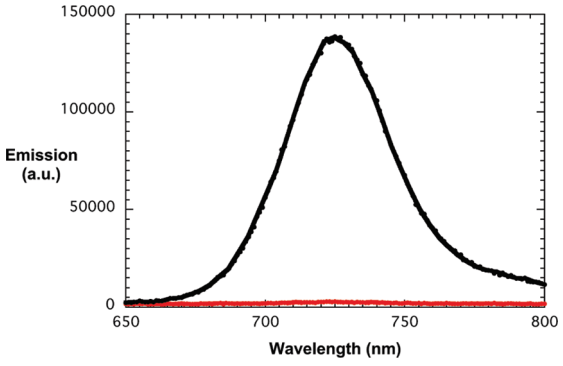

Figure 8. Room temperature steady-state fluorescence spectra of [1] (black spectrum) and f-SWNT [5] (red spectrum) in DMF that exhibit the same optical density at the 450 nm excitation wavelength.

maxima at 460, 493, and 860 nm as well as minima at 650 and 703 nm, as shown in Figure 9. The maxima at 460, 493, and 860 nm correlate to singlet−singlet transitions, while the minimum is due to the depletion of the ground state and reflects consumption of the

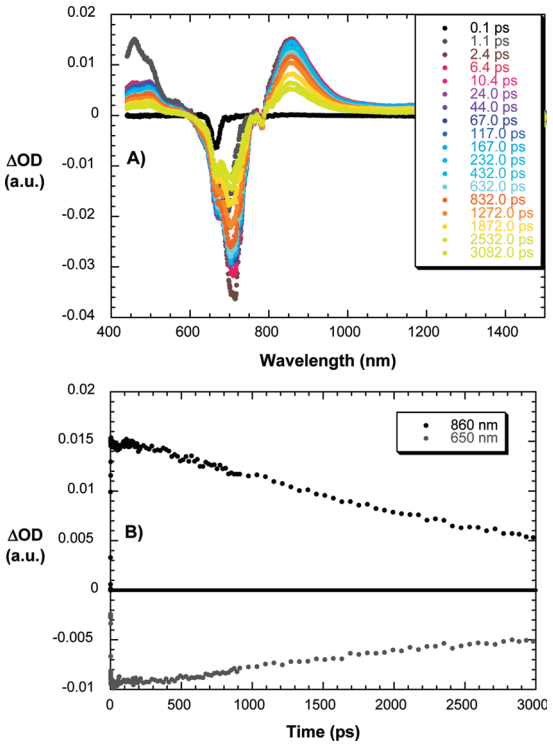

Figure 9. (A) Differential absorption spectra (visible and near-infrared) obtained upon femtosecond laser flash photolysis (700 nm) of [1] in DMF with several time delays between 0 and 3082 ps at room temperature (see figure legend for details). (B) Time-absorption profiles of the spectra shown above at 650 and 860 nm monitoring the singlet excited-state formation and decay.

ground state/state filling. Intersystem crossing to the corresponding triplet manifold is the fate of singlet excited state. A multiwavelength analysis, for which an example is shown in Figure 9, gives rise to an intersystem crossing rate constant of 3.7×10^8 s^{-1}.

Important for further laser flash photolysis studies is information concerning the absorption features of the one electron oxidized fluorophore radical cation. To this end, pulse radiolysis experiments were carried out. Oxidation of fluorophore [**1**] in oxygenated dichloromethane by radiolytically generated radical anions lead to differential absorption changes shown in Figure 10, which were corroborated by spectroelectrochemistry, where we applied an oxidative potential of 1.3 V *vs* a Ag wire. The differential absorption spectra of the oxidized reference fluorophore [**1**] include minima at 469 and 701 nm, a maximum at 564 nm, and a broad maximum at 791 nm (Figure 11).

When analyzing the differential absorption changes of f-SWNTs [**5**] in the visible and infrared (*i.e.*, 400−900 nm), transient peaks, which are centered at 460 and 855 nm, are formed during the initial stage (*i.e.*, from 0 to 2 ps). Based on the similarity with the features seen upon exciting [**1**], we conclude the formation of the fluorophore singlet excited state. In the near-infrared (*i.e.*, 900−1400 nm) a broad bleach evolves, which is an indicator for photoexcited SWNT. The singlet

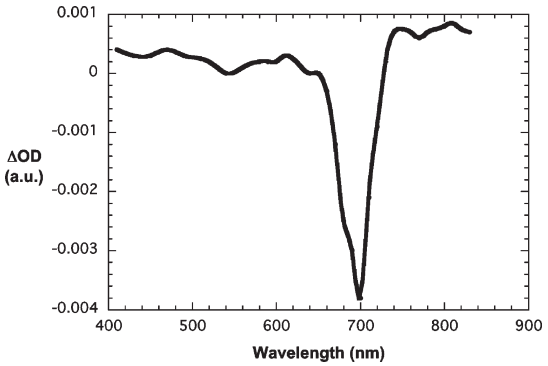

Figure 10. Differential absorption changes following pulse radiolytic oxidation of [1] in oxygenated dichloromethane with $^{\bullet}OOCH_2Cl$ or $^{\bullet}OOCHCl_2$.

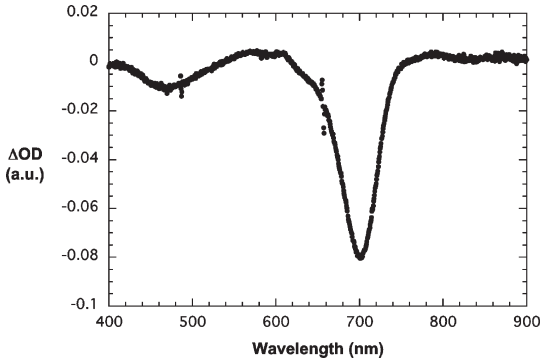

Figure 11. Differential absorption changes following electrochemical oxidation of [1] in dichloromethane at an applied potential of 1.3 V *vs* Ag wire.

excited state characteristics of [**1**] decay all throughout the visible and the near-infrared over the next 10 ps. In parallel with the singlet excited state decay, a broad absorption ranging from 750 to 1150 nm and maximizing at 820 nm emerges (Figure 12). The broad 750−1150 nm feature correlates well with the signature of the one electron oxidized radical cation of [**1**]. On the other hand, differential absorption changes noted upon pulse radiolytic, electrochemical, chemical, and photochemical reduction of pristine SWNT are predominantly located in the near-infrared.[22] As the absorption spectra of f-SWNT [**4**] and [**5**] do not feature distinct transitions between van Hove singularities, the one electron reduced SWNT radical anion is likely to be a broad bleach or to remain spectroscopically invisible to us. In fact, at time delays of around 10 ps, that is, at which the radical cation formation of [**1**] is completed, a broad bleach centered at around 1250 nm is seen. Taken the formation of the one electron oxidized fluorophore radical cation and the broad bleach of SWNT centered transitions into concert, we reach the conclusion that the radical ion pair state is successfully formed.

Upon photoexcitation of [**1**], a lifetime of more than 3 ns has been determined from a multiwavelength analysis, while when attached to f-SWNTs [**5**] a lifetime analysis at 460, 750, 855, and 1250 nm reveals a value of

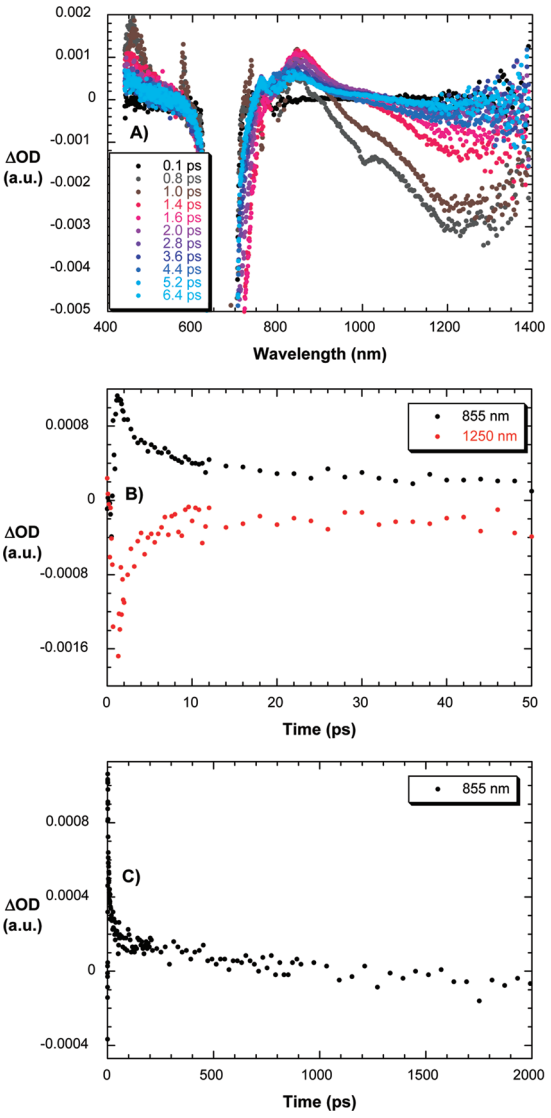

Figure 12. (A) Differential absorption spectra (visible and near-infrared) obtained upon femtosecond laser flash photolysis (700 nm) of f-SWNT [5] in DMF with several time delays between 0 and 6.4 ps at room temperature (see figure legend for details). (B) Time-absorption profiles of the spectra shown above 855 and 1250 nm monitoring the charge separation. (C) Time-absorption profiles of the spectra shown above 1250 nm monitoring the charge recombination.

5.9 ps (see time absorption profile of Figure 12). Moreover, for the subsequently formed maximum of the one electron oxidized fluorophore and the broad bleach of one electron reduced SWNT, a lifetime of 1.2 ns was derived. In summary, the aforementioned supports the presence of a short-lived excited state that transforms into a longer-lived radical ion pair state.

CONCLUSIONS

We have demonstrated the preparation of a novel donor−acceptor material, consisting of a red/NIR absorbing boron azadipyrromethene donor covalently attached to a highly functionalized SWNT acceptor, where successful purification and covalent functionalization

were demonstrated by a number of spectroscopic/microscopic techniques. The electronic interactions between the donor and the SWNT have been confirmed by means of absorption and fluorescence spectroscopies, followed by transient absorption measurements, which verified efficient electron transfer from the photoexcited boron azadipyrromethene to the SWNT. The lifetime of the resulting radical ion pair state has been determined as 1.2 ns, which renders our electron donor−acceptor conjugate as a promising building block in future photovoltaic applications.

METHODS

Materials. Raw HiPco SWNTs were purchased from Unidym, Inc. (lot no. R1921). Reagents and solvents were purchased as reagent/spectroscopic grade from Fisher Scientific Ireland Ltd. or Sigma-Aldrich Ireland and Germany and used without further purification.

Deprotection of [1]. An 8 mg quantity of boc-protected fluorophore [**1**] (synthesis previously described)[27] was dissolved in 2 mL of dichloromethane. A 0.2 mL aliquot of trifluoroacetic acid was slowly added, and the reaction mixture was stirred at room temperature for 2 h. Saturated aqueous $NaHCO_3$ was added, and the resulting suspension extracted with dichloromethane (2×15 mL). The combined organic phases were washed with water, dried over Na_2SO_4, evaporated to dryness, and directly used for conjugation to f-SWNTs [**3**].

Synthesis of p-SWNTs [3]. A 101 mg quantity of raw SWNTs was dispersed in 7.9 M HNO_3 (340 mL) by sonication at maximum power for 5 min and subsequently at minimum power for 10 min. The mixture was then stirred under reflux at 100 °C for 4 h and quenched with ice. The dispersion was then filtered through a Millipore system (0.2 μm Isopore filter) and washed with distilled water until the filtrate ran neutral. The wet solid was transferred to a Teflon tub, dispersed in 2 M NaOH by sonication at maximum power for 5 min, and subsequently stirred overnight at 100 °C under a nitrogen atmosphere. The mixture was cooled to room temperature, filtered through over an Isopore filter, and washed with a further 200 mL of 2 M NaOH. The solid was washed with distilled water until the filtrate pH became neutral, and the sample was subjected to the NaOH treatment one additional time. Following filtration the wet solid was dispersed in 10% H_2O_2 by sonication at maximum power for 5 min and subsequently stirred for 1 h at 100 °C. The dispersion was quenched with ice, filtered over an Isopore filter, and washed with copious amounts of distilled water. The solid was subsequently subjected to a final NaOH treatment and filtered, and the solid was washed with 200 mL 2 M NaOH, distilled water until neutral pH, 200 mL of 1 M HCl, and distilled water until neutral pH, respectively. The wet solid was redispersed in distilled water and freeze dried to afford 23 mg of black solid (yield: 23%).

Synthesis of f-SWNTs [4]. A 12.2 mg quantity of p-SWNTs [**2**] was dispersed in 50 mL *N*-methyl-2-pyrrolidone (NMP) by sonication for 20 min at full power. Following addition of 4-aminobenzoic acid (275 mg, 2 mmol, 2 eqe C), the reaction mixture was put under a nitrogen atmosphere. The reaction mixture was stirred overnight at 70 °C, following addition of isoamyl nitrite (400 μL, 3 mmol, 3 eqe) *via* syringe. After cooling to room temperature, the mixture was briefly sonicated to redisperse the sample and was then filtered through a 0.2 μm fluoropore FG filter, washing with NMP until the filtrate ran clear. The sample was redispersed in NMP (50 mL), and the entire procedure was repeated an additional two times. Finally the solid was washed with methanol and dried under vacuum to afford 13 mg of black solid.

Synthesis of f-SWNTs [5]. A 10.4 mg quantity of f-SWNTs [**3**] was dispersed in thionyl chloride by sonication at maximum power for 10 min. The mixture was subsequently refluxed at 70 °C under a nitrogen atmosphere for 48 h. The dispersion was filtered through a 0.2 μm fluoropore FG filter, washed with dry THF, and directly redispersed in dry THF (50 mL) by brief sonication under a nitrogen atmosphere. A 60 μL aliquot of dry triethylamine, followed by compound [**1**] dissolved in 5 mL of dry THF, was syringed into the reaction mixture, respectively. The mixture was subsequently stirred for 15 h at 80 °C under a nitrogen atmosphere. The mixture was allowed to come to room temperature and was subsequently dispersed in DMSO (200 mL) by brief sonication. The dispersion was filtered through a 0.2 μm fluoropore FG filter and washed with 1% acetic acid in ethanol (150 mL), ethanol, methanol, THF, and methanol, respectively, with sonication following each solvent washing step.

Sample Characterization. Micro-Raman scattering measurements were performed at room temperature in the backscattering geometry using RENISHAW 1000 micro-Raman system equipped with a CCD camera and a Leica microscope. An 1800 line mm^{-1} grating was used for all measurements, providing a spectral resolution of ± 1 cm^{-1}. As an excitation source, the Ar^+ laser (457 nm) was used. Measurements were taken with 10 s of exposure time and 4 accumulations. The laser spot was focused on the sample surface using a 50x objective with short-focus working distance. Raman spectra were collected at numerous spots on the sample and recorded with a Peltier cooled CCD camera. The data was collected and analyzed with Renishaw Wire and GRAMS software.

XPS measurements were performed in a VERSAPROBE PHI 5000 from Physical Electronics, equipped with a monochromatic Al Kα X-ray source with a highly focused beam size, which can be selected from 10 to 300 μm. The energy resolution was 0.6 eV. For the compensation of built up charge on the sample surface during the measurements, a dual beam charge neutralization composed of an electron gun ($\sim$1 eV) and the argon ion gun ($\leq$10 eV) was used.

All FTIR spectra were measured in the solid state on a PerkinElmer FTIR spectrometer spectrum 100 with a universal ATR sampling accessory (diamond/ZnSe crystal). The spectra for organic compounds and functionalized SWNTs were recorded at 36 and 256 scans, respectively, with a 4 cm^{-1} resolution.

The photophysical measurements were performed at room temperature and ambient conditions. Steady-state absorption spectra were measured by a Cary5000 (Varian) two-beam spectrometer.

NIR-PL studies were carried out in a LOT ORIEL Nanospectralyzer NS1 at three different excitation wavelengths (785, 683, and 638 nm). Dispersions of SWNTs in aqueous SDBS were prepared in Milli-Q water with an initial nanotube concentration of 2×10^{-2} mg/mL and with a SWNTs/SDBS mass ratio of 1:25. Nanotubes and SDBS were precisely weighted and dispersed in Milli-Q water by both sonic tip (2 min) and sonic bath (6 h) treatments. The dispersions were centrifuged at 4000 rpm for 90 min, and all optical measurements were carried out on the supernatants in a 1 cm quartz cells.

AFM topographic images were collected in semicontact mode with an NT-MDT inverted configuration system. Silicon tips with reflectance gold coated on the back, tip apex radius 10 nm, force constant 2 N/m, and frequency 170 kHz were used. The data were collected and analyzed with NT-MDT Nova software. Samples were prepared by dispersing the nanotubes in high-purity DMF by sonication, spray coated onto freshly cleaved mica substrates, and dried overnight in oven at 90 °C.

Emission spectra were recorded by using a FluoroMax-P (HORIBA Jobin Yvon). NIR emission spectra were measured by a Fluorolog spectrometer (HORIBA Jobin Yvon). Here, the optical detection was performed by a Symphony InGaAs array in combination with an iHR320 imaging spectrometer. The samples were excited by a 450 W xenon lamp. Time-correlated

single photon counting (TCSPC) spectra were taken with a Fluorolog system (HORIBA Jobin Yvon). The sample was excited by a NanoLED-650 L (peak wavelength 647 nm), and the signal was detected by a Hamamatsu MCP photomultiplier (type R3809U-50). The time profiles were recorded at the emission maximum.

Femtosecond transient absorption studies were performed using an amplified Ti:sapphire laser system (SHG, CPA 2001, Clark-MXR, Inc.) for creating 700 nm laser pulses (200 nJ) by a NOPA (Clark-MXR, Inc.). For the detection we used a Helios TAPPS from Ultrafast Inc.

Electrochemical measurements were carried out by using a HEKA elektronik HEKA 510 potentiostat/galvanostat with a glassy carbon working electrode, a Pt wire counter electrode, and a Ag wire reference electrode. Potentials were measured *vs* Fc/Fc^{+} in deoxygenated samples.

Spectroelectrochemical measurements were performed on an analytic jena SPECORD S 600 diode array spectrophotometer combined with a HEKA elektronik HEKA 28DD5 potentiostat/galvanostat with a Pt gauze working electrode, a Pt wire counter electrode, and a Ag wire reference electrode.

Acknowledgment. This work was supported by Science Foundation Ireland (PIYRA 07/YI2/I1052) and the European Commission under framework 7. DOS/MT acknowledges the Irish Research Council for Science, Engineering, and Technology for financial support. Funding also provided by DFG (GU 517/4-2 and Cluster of Excellence EAM).

Supporting Information Available: Supplementary figures, schemes synthetic, and calculations for the estimation of functionalization efficiency. This material is available free of charge *via* the Internet at http://pubs.acs.org.

REFERENCES AND NOTES

1. Kamat, P. V. Meeting the Clean Energy Demand: Nanostructure Architectures for Solar Energy Conversion. *J. Phys. Chem. C* **2007,** *111*, 2834–2860.
2. Osterloh, F. E. Inorganic Materials as Catalysts for Photochemical Splitting of Water. *Chem. Mater.* **2008,** *20*, 35–54.
3. Gunes, S.; Neugebauer, H.; Sariciftci, N. S. Conjugated Polymer-Based Organic Solar Cells. *Chem. Rev.* **2007,** *107*, 1324–1338.
4. Georgakilas, V.; Kordatos, K.; Prato, M.; Guldi, D. M.; Holzinger, M.; Hirsch, A. Organic Functionalization of Carbon Nanotubes. *J. Am. Chem. Soc.* **2002,** *124*, 760–761.
5. Del Canto, E.; Flavin, K.; Natali, M.; Perova, T.; Giordani, S. Functionalization of Single-Walled Carbon Nanotubes with Optically Switchable Spiropyrans. *Carbon* **2010,** *48*, 2815–2824.
6. Flavin, K.; Chaur, M. N.; Echegoyen, L.; Giordani, S. Functionalization of Multilayer Fullerenes (Carbon Nano-Onions) using Diazonium Compounds and "Click" Chemistry. *Org. Lett.* **2010,** *12*, 840–843.
7. Sharma, R.; Baik, J. H.; Perera, C. J.; Strano, M. S. Anomalously Large Reactivity of Single Graphene Layers and Edges toward Electron Transfer Chemistries. *Nano Lett.* **2010,** *10*, 398–405.
8. Sgobba, V.; Guldi, D. M. Carbon Nanotubes-Electronic/Electrochemical Properties and Application for Nanoelectronics and Photonics. *Chem. Soc. Rev.* **2009,** *38*, 165–184.
9. Guldi, D. M.; Rahman, A.; Sgobba, V.; Ehli, C. Multifunctional Molecular Carbon Materials - From Fullerenes to Carbon Nanotubes. *Chem. Soc. Rev.* **2006,** *35*, 471–487.
10. Ebbesen, T. W.; Lezec, H. J.; Hiura, H.; Bennett, J. W.; Ghaemi, H. F.; Thio, T. Electrical Conductivity of Individual Carbon Nanotubes. *Nature* **1996,** *382*, 54–56.
11. Treacy, M. M. J.; Ebbesen, T. W.; Gibson, J. M. Exceptionally High Young's Modulus Observed for Individual Carbon Nanotubes. *Nature* **1996,** *381*, 678–680.
12. Baughman, R. H.; Zakhidov, A. A.; de Heer, W. A. Carbon Nanotubes - The Route Toward Applications. *Science* **2002,** *297*, 787–792.
13. Herranz, M. A.; Martin, N.; Campidelli, S. P.; Prato, M.; Brehm, G.; Guldi, D. M. Control Over Electron Transfer in Tetrathiafulvalene-Modified Single-Walled Carbon Nanotubes. *Angew. Chem., Int. Ed.* **2006,** *45*, 4478–4482.
14. Guldi, D. M.; Marcaccio, M.; Paolucci, D.; Paolucci, F.; Tagmatarchis, N.; Tasis, D.; Vazquez, E.; Prato, M. Single-Wall Carbon Nanotube-Ferrocene Nanohybrids: Observing Intramolecular Electron Transfer in Functionalized SWNTs. *Angew. Chem., Int. Ed.* **2003,** *42*, 4206–4209.
15. Jang, S. R.; Vittal, R.; Kim, K. J. Incorporation of Functionalized Single-Wall Carbon Nanotubes in Dye-Sensitized TiO_2 Solar Cells. *Langmuir* **2004,** *20*, 9807–9810.
16. Li, H. P.; Martin, R. B.; Harruff, B. A.; Carino, R. A.; Allard, L. F.; Sun, Y. P. Single-Walled Carbon Nanotubes Tethered with Porphyrins: Synthesis and Photophysical Properties. *Adv. Mater.* **2004,** *16*, 896–900.
17. Campidelli, S.; Sooambar, C.; Diz, E. L.; Ehli, C.; Guldi, D. M.; Prato, M. Dendrimer-Functionalized Single-Wall Carbon Nanotubes: Synthesis, Characterization, and Photoinduced Electron Transfer. *J. Am. Chem. Soc.* **2006,** *128*, 12544–12552.
18. Liu, Z. B.; Tian, J. G.; Guo, Z.; Ren, D. M.; Du, T.; Zheng, J. Y.; Chen, Y. S. Enhanced Optical Limiting Effects in Porphyrin-Covalently Functionalized Single-Walled Carbon Nanotubes. *Adv. Mater.* **2008,** *20*, 511–515.
19. Palacin, T.; Le Khanh, H.; Jousselme, B.; Jegou, P.; Filoramo, A.; Ehli, C.; Guldi, D. M.; Campidelli, S. Efficient Functionalization of Carbon Nanotubes with Porphyrin Dendrons via Click Chemistry. *J. Am. Chem. Soc.* **2009,** *131*, 15394–15402.
20. Ni Mhuircheartaigh, E. M.; Giordani, S.; Blau, W. J. Linear and Nonlinear Optical Characterization of a Tetraphenylporphyrin-Carbon Nanotube Composite System. *J. Phys. Chem. B* **2006,** *110*, 23136–23141.
21. Ballesteros, B.; de la Torre, G.; Ehli, C.; Rahman, G. M. A.; Agullo-Rueda, F.; Guldi, D. M.; Torres, T. Single-Wall Carbon Nanotubes Bearing Covalently Linked Phthalocyanines - Photoinduced Electron Transfer. *J. Am. Chem. Soc.* **2007,** *129*), 5061–5068.
22. Ballesteros, B.; Campidelli, S.; de la Torre, G.; Ehli, C.; Guldi, D. M.; Prato, M.; Torres, T. Synthesis, Characterization and Photophysical Properties of a SWNT-Phthalocyanine Hybrid. *Chem. Commun.* **2007,** 2950–2952.
23. Campidelli, S.; Ballesteros, B.; Filoramo, A.; Diaz, D. D.; de la Torre, G.; Torres, T.; Rahman, G. M. A.; Ehli, C.; Kiessling, D.; Werner.; et al. Facile Decoration of Functionalized Single-Wall Carbon Nanotubes with Phthalocyanines via "Click Chemistry. *J. Am. Chem. Soc.* **2008,** *130*, 11503–11509.
24. Mishra, A.; Behera, R. K.; Behera, P. K.; Mishra, B. K.; Behera, G. B. Cyanines During the 1990s: A Review. *Chem. Rev.* **2000,** *100*, 1973–2011.
25. Gorman, A.; Killoran, J.; O'Shea, C.; Kenna, T.; Gallagher, W. M.; O'Shea, D. F. In Vitro Demonstration of the Heavy-Atom Effect for Photodynamic Therapy. *J. Am. Chem. Soc.* **2004,** *126*, 10619–10631.
26. Hall, M. J.; McDonnell, S. O.; Killoran, J.; O'Shea, D. F. A Modular Synthesis of Unsymmetrical Tetraarylazadipyrromethenes. *J. Org. Chem.* **2005,** *70*, 5571–5578.
27. Tasior, M.; O'Shea, D. F. BF2-Chelated Tetraarylazadipyrromethenes as NIR Fluorochromes. *Bioconjugate Chem.* **2010,** *21*, 1130–1133.
28. Palma, A.; Tasior, M.; Frimannsson, D. O.; Vu, T. T.; Meallet-Renault, R.; O'Shea, D. F. New On-Bead Near-Infrared Fluorophores and Fluorescent Sensor Constructs. *Org. Lett.* **2009,** *11*, 3638–3641.
29. Murtagh, J.; Frimannsson, D. O.; O'Shea, D. F. Azide Conjugatable and pH Responsive Near-Infrared Fluorescent Imaging Probes. *Org. Lett.* **2009,** *11*, 5386–5389.
30. McDonnell, S. O.; Hall, M. J.; Allen, L. T.; Byrne, A.; Gallagher, W. M.; O'Shea, D. F. Supramolecular Photonic Therapeutic Agents. *J. Am. Chem. Soc.* **2005,** *127*, 16360–16361.
31. Bahr, J. L.; Tour, J. M. Highly Functionalized Carbon Nanotubes using in situ Generated Diazonium Compounds. *Chem. Mater.* **2001,** *13*, 3823–3824.
32. Strano, M. S.; Dyke, C. A.; Usrey, M. L.; Barone, P. W.; Allen, M. J.; Shan, H. W.; Kittrell, C.; Hauge, R. H.; Tour, J. M.; Smalley, R. E. Electronic Structure Control of Single-Walled

Carbon Nanotube Functionalization. *Science* **2003,** *301*, 1519–1522.
33. Ferrari, A. C.; Robertson, J. Interpretation of Raman Spectra of Disordered and Amorphous Carbon. *Phys. Rev. B: Condens. Matter Mater. Phys.* **2000,** *61*, 14095–14107.
34. Okpalugo, T. I. T.; Papakonstantinou, P.; Murphy, H.; Mclaughlin, J.; Brown, N. M. D. Oxidative Functionalization of Carbon Nanotubes in Atmospheric Pressure Filamentary Dielectric Barrier Discharge (APDBD). *Carbon* **2005,** *43*, 2951–2959.
35. Schmidt, G.; Gallon, S.; Esnouf, S.; Bourgoin, J. P.; Chenevier, P. Mechanism of the Coupling of Diazonium to Single-Walled Carbon Nanotubes and Its Consequences. *Chem.—Eur. J.* **2009,** *15*, 2101–2110.
36. Doyle, C. D.; Rocha, J. D. R.; Weisman, R. B.; Tour, J. M. Structure-Dependent Reactivity of Semiconducting Single-Walled Carbon Nanotubes with Benzenediazonium Salts. *J. Am. Chem. Soc.* **2008,** *130*, 6795–6800.
37. Hirsch, A. Functionalization of Single-Walled Carbon Nanotubes. *Angew. Chem., Int. Ed.* **2002,** *41*, 1853–1859.